Progress In Electromagnetics Research M, Vol. 24, 57–68, 2012

PRELIMINARY RESULTS ON BRAIN MONITORING OF MENINGITIS USING 16 CHANNELS MAGNETIC INDUCTION TOMOGRAPHY MEASUREMENT SYSTEM

H. J. Luo[1,*], W. He[1], Z. Xu[1], and L. Liu[2]

[1]State Key Laboratory of Power Transmission Equipment & System Security and New Technology, the Electrical Engineering College, Chongqing University, Chongqing 400044, China

[2]Chongqing Cancer Institute, Chongqing 400030, China

Abstract—Magnetic induction tomography (MIT) is a contactless measurement technique of biological tissue conductivity. In this study, the differential induced voltage equations are shown in single layer and **n** layers models. The paper describes a 16 channels MIT measurement system with working frequency of 1 MHz, which can image the plan of low conductivity object. According to physical experiments, the sensitivity is about $0.29^\circ/\mathrm{S}\cdot\mathrm{m}^{-1}$, and the maximum shift of the phase noise is 0.08°. Some preliminary clinical experiments were done, including 2 cases of meningitis and 5 cases of brain normal patients. The comparison of all the measured values shows that all values are smaller than 1.7° in the brain normal cases, but the values of meningitis cases are more than 2°, higher than those of brain normal patients. Therefore, the MIT measurement system has great application prospect in dynamically monitoring the brain diseases.

1. INTRODUCTION

Magnetic induction tomography (MIT) is a contactless measurement of biological tissue conductivity imaging technique [1, 2], based on the theory of Faraday's law of electromagnetic induction. The basic principle: when the excitation coil generates the alternating primary magnetic field $\mathbf{B}$, eddy currents are induced into the biological tissue and generates the secondary magnetic field $\mathbf{\Delta B}$ that perturbs the

Received 14 February 2012, Accepted 12 March 2012, Scheduled 21 March 2012

* Corresponding author: Hai Jun Luo (lhj19830330@126.com).

primary magnetic field in the vicinity. The detection coils can find these perturbations. The induced voltage and conductivity distribution have a close relationship. Conductivity distribution can be imaged by the reconstruction algorithm [3–5]. In summary, this imaging technique has very good application prospect in biomedical noninvasive imaging and great potential in medical diagnostics, especially for brain imaging and monitoring [6].

In recent years, the study of MIT has become popular in the medical field, and some MIT measurement systems have been reported. Griffiths et al. introduced a single channel MIT system working at 10 MHz [7]. A system was published by Korjenevsky et al. containing 16 excitation and detector coils, and 16 modules (oscillators and receivers) [8]. Scharfetter et al. [9] showed a MIT system working at 150 kHz which uses a group of planar gradiometer coils and high-precision phase detector to minimize the influence of the primary magnetic field. Watson et al. reported a 16-channel, electronically-switched MIT system operating at 10 MHz and applying phase-sensitive detection for signal demodulation [10]. Riedel et al. described a multichannel planar-array MIT system with a 2×2 planar matrix of axial gradiometers [11, 12]. Rosell-Ferrer (2006) proposed a multi-frequency 14-channel MIT system using planar gradiometers [13]. But these systems did not provide any clinical experimental results. Based on our system, some sensitivity experiments, stability experiments, and clinical experiments are carried out.

2. THE FORWARD PROBLEM

In forward problem, analytical solution is a fundamental method. For simplifying calculation, the solving area is divided into 4 areas in a single layer model. The electrical characteristic of each area is the same. The magnetic vector potential A_i $(i = 1, 2, 3, 4)$ of each area was reported by Dodd and Deeds [14] and Lei [15]. Due to two detecting coils located in the 3rd and 4th areas, the two magnetic vector potentials (A_3, A_4) are presented as follow:

$$A_3 = \frac{1}{2}\mu_0 I\rho' \int_0^\infty J_1(\lambda\rho) J_1(\lambda\rho') e^{-\lambda z'} \left(e^{\lambda z} + \alpha e^{-\lambda z}\right) \cdot d\lambda \quad (1)$$

$$A_4 = \frac{1}{2}\mu_0 I\rho' \int_0^\infty J_1(\lambda\rho) J_1(\lambda\rho') \left(e^{\lambda z'} + \alpha e^{-\lambda z'}\right) e^{-\lambda z} \cdot d\lambda \quad (2)$$

$$\begin{aligned} \alpha &= \frac{j\omega\mu_0\sigma\left(1 - e^{2uc}\right)}{-(\lambda - u)^2 + (\lambda + u)^2 \cdot e^{2uc}} \\ u &= \sqrt{\lambda^2 + (\omega\mu_0\sigma)^2} \end{aligned} \quad (3)$$

where A_3 is the magnetic vector potential in the 3rd area, A_4 the magnetic vector potential in the 4th area, ω the angular frequency, μ_0 the permeability in the vacuum, ρ the radius of detecting coil, ρ' the radius of exciting coil, $J_1()$ the primal Bessel function, λ the separation constant, and σ the conductivity of the measured object.

In this study, the gradiometer coils were used. The differential induced voltage of two detecting coils is presented as follow:

$$\begin{aligned} V &= -j\omega \cdot 2\pi r \cdot [A_4(\rho, z_1) - A_3(\rho, z_2)] \\ &= -j\omega\pi\rho\mu_0 I\rho' \cdot \int_0^\infty J_1(\lambda\rho) J_1\left(\lambda\rho'\right) \\ &\quad \left[\left(e^{\lambda z'} + \alpha e^{-\lambda z'}\right) e^{-\lambda z_1} - e^{-\lambda z'}\left(e^{\lambda z_2} + \alpha e^{-\lambda z_2}\right)\right] d\lambda \\ &= -j\omega\pi\rho\mu_0 I\rho' \cdot \int_0^\infty J_1(\lambda\rho) J_1\left(\lambda\rho'\right) \\ &\quad \left[e^{\lambda(z'-z_1)} - e^{\lambda(z_2-z')} + \alpha\left(e^{-\lambda(z'+z_1)} - e^{-\lambda(z'+z_2)}\right)\right] d\lambda \end{aligned} \quad (4)$$

where V is the differential induced voltage of two detecting coil in a single layer model and z' the distance between the exciting coil to the phantom. z_1 and z_2 are respectively the distances between detecting coils L2, L3 and the phantom.

If the detecting coils L2 and L3 are completely symmetrical on the exciting coil L1, then

$$z_1 - z' = z' - z_2 \quad (5)$$

Equation (5) is substituted into Equation (4). When the primary magnetic field is completely offset, the differential induced voltage V is then:

$$V = -j\omega\pi\rho\mu_0 I\rho' \cdot \int_0^\infty J_1\left(\lambda\rho\right) J_1\left(\lambda\rho'\right) \cdot \alpha\left(e^{-\lambda(z'+z_1)} - e^{-\lambda(z'+z_2)}\right) \cdot d\lambda \quad (6)$$

In the multi-layer model of forward problem, we assume that the model has **n** layers with equal thickness, as shown in Figure 1.

The output voltage of the sensor is the sum of the induced voltages of all layers, presented as follow:

$$\begin{aligned} V' &= V_1 + V_2 + \cdots\cdots + V_n \\ &= -j\omega\pi\rho\mu_0 I\rho' \cdot \int_0^\infty J_1(\lambda\rho) J_1\left(\lambda\rho'\right) \cdot \left[n \cdot \left(e^{\lambda(Z'-Z_1)} - e^{\lambda(Z_2-Z')}\right)\right. \\ &\quad \left. + \sum_{i=1}^{n} a_i \cdot \left(e^{-\lambda(Z'+Z_1+2(i-1)c)} - e^{-\lambda(Z'+Z_2+2(i-1)c)}\right)\right] \cdot d\lambda \end{aligned} \quad (7)$$

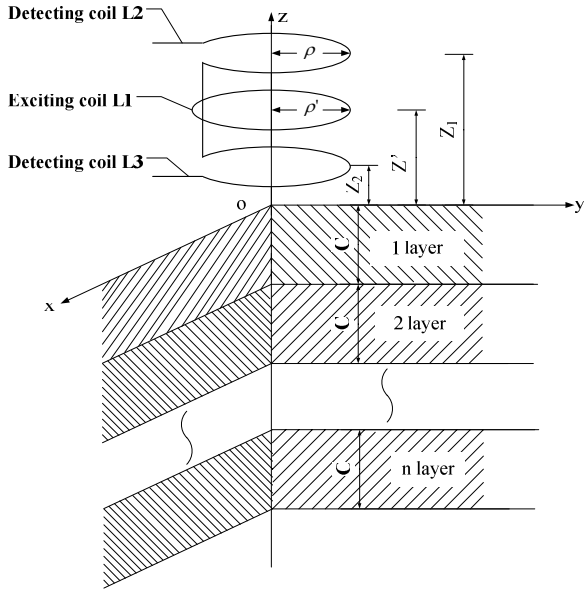

Figure 1. Multi-layer biological tissue model under one sensor.

$$\begin{aligned} \alpha_i &= \frac{j\omega\mu_0\sigma_i(1-e^{2u_ic})}{-(\lambda-u_i)^2+(\lambda+u_i)^2\cdot e^{2u_ic}} \\ u_i &= \sqrt{\lambda^2+(\omega\mu_0\sigma_i)^2} \end{aligned} \tag{8}$$

When the primary magnetic field is completely offset, V' can be expressed:

$$\begin{aligned} V' \;=\; & -j\omega\pi\rho\mu_0 I\rho'\cdot\int_0^\infty J_1(\lambda\rho)J_1(\lambda\rho') \\ & \cdot\left[\sum_{i=1}^{n}\alpha_i\cdot\left(e^{-\lambda(z'+z_1+2(i-1)c)}-e^{-\lambda(z'+z_2+2(i-1)c)}\right)\right]\cdot d\lambda \end{aligned} \tag{9}$$

where V' is the differential induced voltage of two detecting coils in a multi-layer model and $\mathbf{C}$ the thickness of each layer.

3. SYSTEM AND METHODS

When magnetic induction tomography is used in medical image, due to the low conductivity of biological tissue, a high accuracy phase measurement system is necessary. To increase the phase accuracy, the gradiometer coils are used in the magnetic induction measurement

system [11–13]. The coaxial gradiometer coils consist of two detection coils and an excitation coil. The two detection coils are located on the two sides of the excitation coil, shown in Figure 2(a). The preamplifier board and power amplifier board are fixed by three plastic columns above the coils, so as to reduce the distance from sensor to the preamplifier circuit and improve the SNR (Signal Noise Rate) of the sensor.

As shown in Figure 2, two illustrations describe the construction of a single sensor. The sensor is composed of two detection coils, one excitation coil, preamplifier board, and power amplifier board. The excitation and detection coils are spiral coil based on single-sided PCB board with 2 mm thickness. The width of spiral copper wire is 0.15 mm, diameter 25 mm, and 23 turns. The distance from the excitation coil to the detection coils is 8 mm. The distance from the power amplifier board to the detection coil is 44 mm. The distance from the power amplifier board to the preamplifier board is 8 mm. They are fixed on a plastic substrate.

The MIT measurement system has 16-channel sensors. Their arrangement is shown in Figure 3(a). Eight sensors are fixed in the first circle and the other eight in the second circle. Two groups of sensors staggered on in the hood. The reality sensor hood is shown

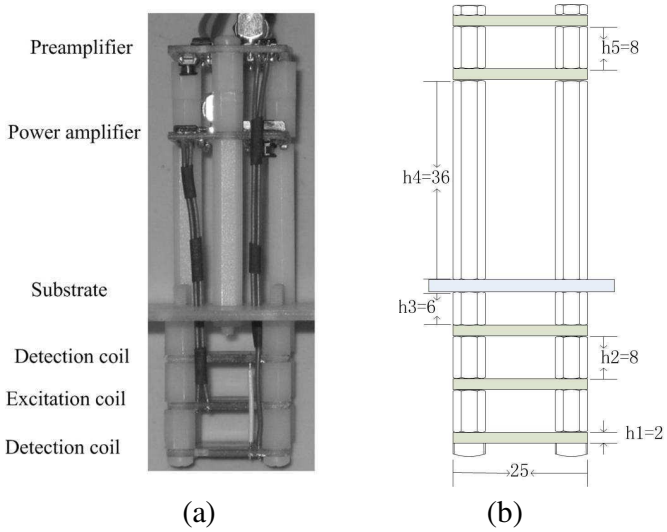

Figure 2. (a) Sensor unit. (b) Schematic of the sensor from the side. (All units are in mm).

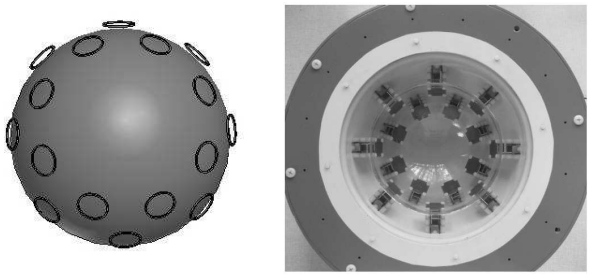

(a) (b)

Figure 3. (a) The diagram of the sensor arrangement. (b) The sensor from the top.

in Figure 3(b). A hemispherical and transparent container is used to simulate a simple human brain model. The 16 measurement sensor units are sealed into space between the two different radiuses bowls, which can make sure the same environment. The radius of the small one is 75 mm to suit the children's brain. The distance between the two bowls is 45 mm for placing the sensors.

The 16 sensor units independently measure data alternately, i.e., the 16 sensors work by turns in a complete measurement. For each excitation coil, only the two coaxial detection coils are available. The measurement method is divided into two steps: Firstly, the system collects the first group of phase data in the air taken as a reference value. Secondly, the measurement of the target object obtain the second group of phase data. The differences between two groups of data are projected into a 2-D imaging plane.

The inverse distance weighted (IDW) interpolation algorithm is applied to obtain other data. The basic principle is shown as following. Assuming that Z_i $(i = 1, 2, 3 \ldots n)$ are the data of measured point and that Z_P expresses the value of interpolation point calculated by the IDW algorithm. The magnitude of weight relates to the distance from the interpolation point to the measuring point and is the reciprocal of kth $(0 \leq k \leq 2)$ power of the distance [16].

$$Z_P = \frac{\sum_{i=1}^{n} \frac{Z_i}{d_i^k}}{\sum_{i=1}^{n} \frac{1}{d_i^k}} \tag{10}$$

where d_i is the distance between the interpolation point to the ith measuring point.

4. RESULTS

The excitation current was 30 mA and the frequency 1 MHz. The phantom was placed coaxially 5 mm from the bottom of the sensor unit. Before the experiment, the system must work 10 minutes in advance to avoid the phase drift from temperature rising because of system powering up. The perturbations of magnitude and phase in the detection signal are recognized as the conductivity changes, but phase change has much higher value than magnitude change, so the magnitude change is missed [17].

4.1. Physical Experiments

The value of sensitivity experiment is obtained by a single-channel gradiometer system. The distilled water and *NaCl* solution are taken as phantoms. The conductivity of distilled water is very low and can be considered as 0 S/m. The experiments were repeated several times at each conductivity point, and the average of the measurement values is taken. As shown in Figure 4, the measured points are focused around the straight line. When the phantom is distilled water (that is 0 S/m), the phase difference is 0.9 degree, which shows the existence

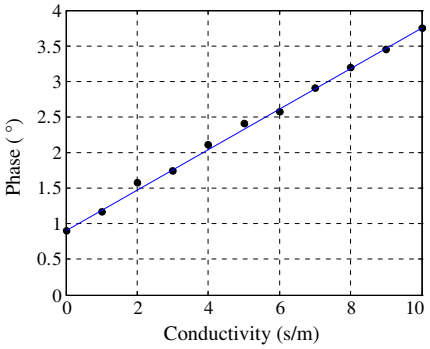

Figure 4. Phase vs. Conductivity. The vertical coordinate is the phase difference between measuring phantom and air(the unit is degree.). The horizontal coordinate is conductivity(the unit is S/m.). The conductivity of NaCl solution increased from 0 S/m to 10 S/m with a step of 1 S/m.

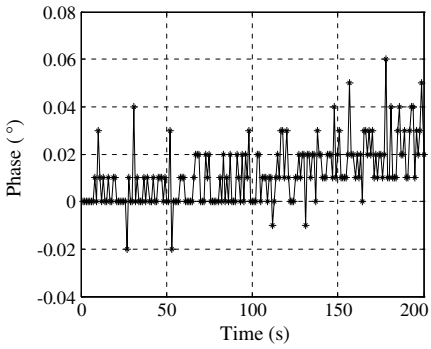

Figure 5. Phase noise. The vertical coordinate is the phase difference between measuring phantom and air (the unit is degree). The horizontal coordinate is time (the unit is s).

of capacitive coupling. When the conductivity of *NaCl* solution is 10 S/m, the phase value is 3.8 degree. With increasing conductivity from 0 S/m to 10 S/m, the phase change was linear, and the maximum change is 2.9 degree. As a result, the sensitivity of phase change is about $0.29°/S \cdot m^{-1}$.

As shown in Figure 5, a series of phase drift values are obtained by subtracting all the phase values from the first measurement phase value in half an hour. The minimum phase drift value is −0.02 degree, and the maximum is 0.06 degree, so the maximum change range is 0.08 degree. According to the above sensitivity and phase drift values, the system can measure the minimum conductivity as 0.27 S/m.

4.2. Clinical Experiments

The present study adhered to the tenets of the Declaration of Helsinki. Additionally, consent was obtained from the parents of the patients. The system is a noninvasive, contactless and very low radiation detection device.

As prototype of the MIT measurement system is shown in Figure 6(a). The measurement of the clinical experiments is divided into two steps: Firstly, the probe hood collects a group of phase data as a reference signal in the air and secondly, measures the second group of data with wearing on the patient's head. Finally, based on the difference between the two groups of data, the imaging result is displayed in the PC using the inverse distance weighted (IDW) interpolation algorithm. Figure 6(b) shows the schematic diagram of clinical experiments. The clinical operation of the system is very simple. The patient is seated under the sensor hood, and then the

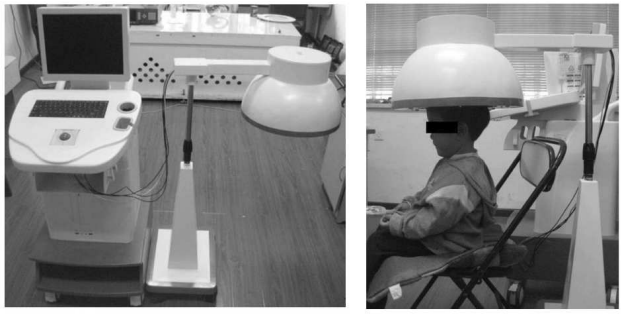

(a) (b)

Figure 6. (a) The MIT measurement system. (b) The schematic diagram of clinical experiments.

patient's head is positioned inside the hood, which takes half a minute.

Using the system, we did the preliminary clinical experiments. Seven cases are detected by the MIT measurement system in Children's Hospital, including 2 mumps with meningitis patients and 5 brain normal patients. The data of clinical experiments are given in Table 1, and further comparison details are shown in Figures 7(a), (b), and Figure 8.

All the measurement data are listed in Table 1. Each column

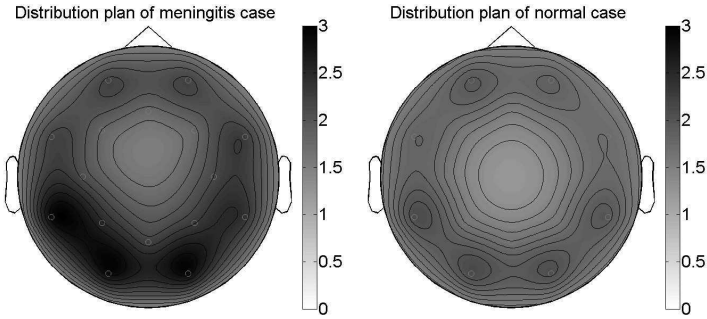

Figure 7. Comparison of the image results for the two different cases. (a) Image of a meningitis patient (case 1). (b) Image of the brain normal (case 3).

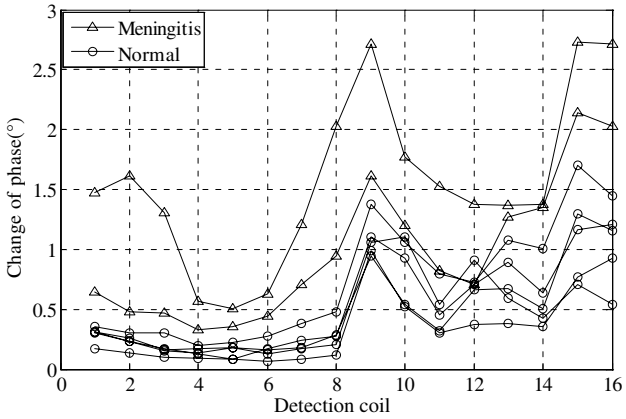

Figure 8. Comparing the phase change of the two kinds of cases. The vertical coordinate is the measurement change of phase, while the horizontal coordinate is the sensor number. Triangular mark lines are meningitis patient's data, and the other are brain normal patient's data.

Table 1. Value of the clinical experiments.

Sensor number	Case 1 ∼ Case 7						
No. 1	1.47	0.65	0.30	0.17	0.31	0.36	0.31
No. 2	1.61	0.48	0.23	0.14	0.23	0.30	0.26
No. 3	1.31	0.47	0.17	0.10	0.15	0.30	0.16
No. 4	0.57	0.33	0.13	0.09	0.14	0.20	0.17
No. 5	0.51	0.36	0.08	0.08	0.18	0.22	0.18
No. 6	0.63	0.44	0.17	0.07	0.16	0.28	0.13
No. 7	1.21	0.71	0.24	0.08	0.18	0.38	0.17
No. 8	2.03	0.95	0.28	0.12	0.29	0.48	0.21
No. 9	2.71	1.61	1.10	0.99	0.95	1.38	1.06
No. 10	1.77	1.20	0.93	0.52	0.54	1.06	1.10
No. 11	1.53	0.82	0.45	0.30	0.32	0.80	0.54
No. 12	1.38	0.71	0.71	0.37	0.66	0.73	0.91
No. 13	1.37	1.27	0.89	0.38	0.67	1.08	0.59
No. 14	1.38	1.35	0.64	0.36	0.51	1.01	0.43
No. 15	2.73	2.14	1.17	0.77	1.30	1.70	0.71
No. 16	2.71	2.03	1.21	0.93	1.16	1.45	0.54

Seven cases include 2 mumps with meningitis cases (case 1, case 2) and 5 brain normal cases (case 3, case 4, case 5, case 6, case 7). The table's data are the difference between measurement phase in the air and wearing on the patient's head (Unit: degree).

records 16 sensors data of a certain case. Four sensors' values are more than 2 degrees in case 1, while two sensors' values in case 2. But all values are smaller than 1.7 degrees in the brain normal cases. Therefore, the data of meningitis cases are larger than those of brain normal cases.

According to the values in Table 1, the distribution plans of case 1 and case 3 are imaged as Figures 7(a), (b). When comparing the two planar images, it is visible that there are some shadows in the image of meningitis. The image results can be directly used to select the meningitis patients.

As shown in Figure 8, the different measurement results of the two kinds of cases are clear. The values of meningitis patients are higher than those of brain normal patients. This comparison result shows the worth of studying the dynamic monitoring meningitis with MIT system.

5. DISCUSSIONS

In the paper, the multi-channel MIT measurement system is described. The principle, construction and working method of the system are also shown. In the study, a series of experiments were carried out using the multi-channel MIT measurement system. The study and analysis described above show:

1) The system has a better sensitivity of phase change using the gradiometer coils, about $0.29°/\mathrm{S} \cdot \mathrm{m}^{-1}$. The maximum change range of phase noise is 0.08°.

2) According to the results of preliminary clinical experiments, the system can show the difference between the meningitis and normal cases. The point is of powerful significance in the medical applications.

In the paper, we apply inverse distance weighted (IDW) interpolation algorithm to calculate the data in the imaging region, but the algorithm is rough. The reconstruction algorithm needs future study.

ACKNOWLEDGMENT

This work was supported by The Fundamental Research Funds for the Central Universities (Project No. CDJZR10150021).

REFERENCES

1. Xu, Z., W. He, C.-H. He, and Z.-L. Zhang, "Study on the principles and system of measurement biological tissue conductivity with magnetic induction method," *Chinese Journal of Scientific Instrument*, Vol. 29, No. 9, 1878–1882, 2008.
2. He, W., C.-Y. Luo, and Z. Xu, *Electrical Impedance Tomography Principle*, Science Press, Beijing, 2009.
3. Ma, L., H.-Y. Wei, and M. Soleimani, "Pipelines inspection using magnetic induction tomography based on a narrowband pass filtering method," *Progress In Electromagnetics Research M*, Vol. 23, 65–78, 2012.
4. Wei, H.-Y. and M. Soleimani, "Three-dimensional magnetic induction tomography imaging using a matrix free Krylov subspace inversion algorithm," *Progress In Electromagnetics Research*, Vol. 122, 29–45, 2012.
5. Chen, Y.-Y., X. Wang, Y. Lv, and D. Yang, "An image reconstruction algorithm based on Tikhonov and variation regularization for magnetic induction tomography," *Journal of Northeastern University*, Vol. 32, No. 4, 460–463, 2011.

6. Holder, D. S. and H. Griffiths, "Magnetic induction tomography," *Electrical Impedance Tomography: Methods, History and Applications*, Chapter 8, 213–238, IOP Publishing, 2005.
7. Griffiths, H., W. R. Stewart, and W. Gough, "Magnetic induction tomography: A measuring system for biological tissues," *Annals of the New York Academy of Sciences*, Vol. 873, 335–345, 1999.
8. Korjenevsky, A., V. Cherepenin, and S. Sapetsky, "Magnetic induction tomography: Experimental realization," *Physiol. Meas.*, Vol. 21, No. 1, 89–94, 2000.
9. Scharfetter, H., H. K. Lackner, and J. Rosell, "Magnetic induction tomography: Hardware for multi-frequency measurement in biological tissues," *Physiol. Meas.*, Vol. 22, 131–146, 2001.
10. Watson, S., R. J. Williams, and H. Griffiths, "The Cardiff magnetic induction tomography system," *Proc. Int. Fed. Med. Biol. Eng. EMBEC02*, 116–117, Vienna, Austria, Dec. 4–8, 2002.
11. Riedel, C. H. and O. Dossel, "Planar system for magnetic induction impedance measurement," *4th Conference on Biomedical Applications of Electrical Impedance Tomography*, 23–25, UMIST, Manchester, Apr. 32, 2003.
12. Riedel, C. H., M. Keppelen, S. Nani, and O. Dossel, "Planar system for magnetic induction tomography using a sensor matrix," *Physiol. Meas.*, Vol. 25, 403–411, 2004.
13. Rosell-Ferrer, J., R. Merwa, P. Brunner, and H. Scharfetter, "A multi-frequency magnetic induction tomography system using planar gradiometers: Data collection and calibration," *Physiol. Meas.*, Vol. 27, 271–280, 2006.
14. Dodd, C. V. and W. E. Deeds, "Analytical solutions to eddy-current probe coil problems," *Journal of Applied Physics*, Vol. 39, No. 6, 2829–2838, 1968.
15. Lei, Y.-Z., *Analytic Solution of Harmonic Electromagnetic*, 182–187, Science Press, Beijing, 2000.
16. Wang, K., P.-C. He, Y. Dong, and L. Chen, "The application of cluster analysis and inverse distance weighted interpolation to appraising the water quality of three forks lake," *Procedia Environmental Sciences*, Vol. 10, 2511–2517, 2011.
17. Watson, S., R. J. Williams, H. Griffiths, W. Gough, and A. Morris, "Frequency downconversion and phase noise in MIT," *Physiol. Meas.*, Vol. 23, 189–194, 2002.